Journal of Alloys and Compounds 519 (2012) 129–135

Contents lists available at SciVerse ScienceDirect

Journal of Alloys and Compounds

journal homepage: www.elsevier.com/locate/jallcom

Effect of co-doping of Mg and La on conductivity of ceria

Namrata Singh, Nitish Kumar Singh, Devendra Kumar, Om Parkash*

Department of Ceramic Engineering, Institute of Technology, Banaras Hindu University, Varanasi 221005, India

ARTICLE INFO

Article history:
Received 28 November 2011
Received in revised form
27 December 2011
Accepted 27 December 2011
Available online 5 January 2012

Keywords:
Ceria
Impedance analysis
Ionic conductivity
Solid oxide fuel cells

ABSTRACT

The aim of present investigation is to study the effect of co-doping of lanthanum and magnesium on the ionic conductivity of CeO_2 for its use as a solid electrolyte in the intermediate temperature solid oxide fuel cells (IT SOFC). Attempts have been made to synthesize compositions with $x = 0.075$, 0.07, 0.06, 0.05 and 0.00 and $y = 0.00$, 0.01, 0.03, 0.05 and 0.15 in the system $Ce_{1-x-y}Mg_xLa_yO_{2-x-y/2}$ (CML) by auto-combustion method. X-ray diffraction patterns show that all the samples have fluorite structure similar to undoped ceria. Microstructures of thermally etched samples have been studied by scanning electron microscopy (SEM). In order to evaluate the contributions of grains σ_g, grainboundaries σ_{gb} and electrode–specimen interface to the total conductivity σ_t, use is made of AC impedance analysis. Impedance measurements are made in the frequency range 1 Hz to 1 MHz and temperature range 250–500 °C. The results show that the conductivity of the system increases with increasing lanthanum content. There is no enhancement in conductivity due to co-doping with La and Mg.

1. Introduction

The present challenge of SOFC technology is to develop practical set-up with its operation in intermediate temperature range i.e. 500–700 °C. Yttria-stabilized zirconia (YSZ) is being used currently as a solid electrolyte. Its ionic conductivity is sufficient for its use as a solid electrolyte only at high temperature (900–1000 °C). Further to have compatibility with the electrodes and interconnect, costly materials are required at this high temperature [1]. Research efforts are being made to lower the temperature of operation (500–700 °C) to enable the use of cheap materials for other components of the cell. Fuel cells used in this temperature range are called intermediate temperature solid oxide fuel cells, IT SOFCs. Ceria based electrolytes seem to be highly promising for this [2,3]. Ionic conductivity is closely related to formation of oxygen-vacancies and their migration [4–6]. Ceria (CeO_2) itself is not a good ionic conductor but its ionic conductivity increases significantly with introduction of oxygen vacancies by doping of aliovalent cations in ceria as given below [7]:

$$La_2O_3 \xrightarrow{2CeO_2} 2La'_{Ce} + 3O_o + V_o^{\bullet\bullet} \quad (1)$$

$$MgO \xrightarrow{CeO_2} Mg''_{Ce} + O_o + V_o^{\bullet\bullet} \quad (2)$$

Ceria doped with gadolinia [8], samaria, yttria [2], and calcia [4,9] exhibits high ionic conductivity and these are stable at intermediate temperatures [10]. Ceria-based compounds doped with rare-earth elements give higher oxide ionic conductivity than those doped with other elements [1,2,8]. It has been reported that co-doping gives higher ionic conductivity than the single doping in ceria in the temperature range 500–700 °C. e.g. co-doping of Mg and Sm [11], La and Ca [12], Sm and Ca [13], two rare earths e.g. Sm and Gd [14], Gd and Pr [15], Sm and La [16]. Effect of co-doping of La and Mg has not been studied so far. This system has been investigated in the present work. It is well established, that to get enhanced ionic conductivity, the dopant should be such that strain generated due to radii mismatch is minimum. Since Mg^{2+} is smaller than Ce^{4+} and La^{3+} is larger than Ce^{4+} [18], a combination of these two has been chosen to get a suitable concentration so that the strain is minimum. This is expected to give enhancement in conductivity. Further if these materials are found to exhibit conductivity comparable or better than ceria doped singly or co-doped rare earth ions such as e.g. Sm and Gd then the cost of solid electrolyte will be reduced considerably. A few compositions have been prepared in the system $Ce_{1-x-y}Mg_xLa_yO_{2-x-y/2}$ by auto-combustion method and their electrical conductivity has been studied.

2. Experimental procedure

Powders of $Ce_{1-x-y}Mg_xLa_yO_{2-x-y/2}$ (CML) were synthesized by citrate–nitrate auto-combustion technique. Ammonium ceric nitrate $(NH_4)_2[Ce(NO_3)_6]$ (>99% purity, G.S. Chemical Testing & Allied Industries, New Delhi), lanthanum oxalate $La_2(C_2O_4)_3{\cdot}9H_2O$ (99% purity), magnesium nitrate $Mg(NO_3)_2{\cdot}6H_2O$ (99% purity, Central Drug House (P) Ltd., Mumbai-Delhi), citric acid $C_6H_8O_7{\cdot}H_2O$ (99% purity, Polypharm Private Ltd., Mumbai) were used as starting materials. Lanthanum oxalate was converted into its nitrate with the help of nitric acid. Aqueous solutions of ammonium ceric nitrate, lanthanum nitrate, magnesium nitrate, and citric acid were prepared separately and mixed in appropriate amounts maintaining the citrate to nitrate (C/N) ratio as 0.3 to have a controlled combustion [17]. The mixed

* Corresponding author. Tel.: +91 542 6701791; fax: +91 542 2368428.
E-mail address: oprakash.cer@itbhu.ac.in (O. Parkash).

0925-8388/$ – see front matter © 2012 Elsevier B.V. All rights reserved.
doi:10.1016/j.jallcom.2011.12.137

Table 1
Crystallite size of sintered powders obtained by XRD for compositions CML00, CML01, CML03, CML05 and CML15.

Composition	Crystallite size of sintered sample (nm)
CML00	50
CML01	53
CML03	52
CML05	54
CML15	56

solution was evaporated by heating on a hot plate using a magnetic stirrer at ~200 °C till it became gel. The gel slowly foamed and finally burnt on its own to produce light brown powder. In the combustion mixture, nitrates and citric acid act as oxidants and fuels respectively. The whole process after completion gives rise to yellow-colored powder (ash). The powder (ash) was calcined at 1100 °C for 2 h. The calcined powder was pelletized under a load of 60 kN into cylindrical pellets (diameter ~13 mm, thickness ~2.5 mm). The pellets were sintered at 1350 °C for 4 h.

Powder X-ray diffraction (XRD) patterns of sintered pellets were recorded using Rigaku X-ray diffractometer employing Cu Kα radiation with Ni filter for determination of crystal structure. Theoretical density was calculated from the molecular weight and the unit cell volume (a^3). Experimental density was determined using Archimedes principle. Percentage porosity was calculated from the theoretical and the experimental density. For microstructural studies, sintered pellets were polished using emery papers of grade 1/0, 2/0, 3/0, and 4/0 followed by polishing on a velvet cloth with diamond paste of grade 1/4-OS-475 (HIFIN) and then thermally etched at 1250 °C for 15 min. The samples were coated with gold by sputtering. Micrographs were taken using Inspect S-50, FP 2017/12 Scanning Electron Microscope (SEM). Two probe AC impedance measurements were made on pellets electroded with silver paint using Novocontrol Alpha-A High Performance Frequency Analyzer in the frequency range 1 Hz to 1 MHz and in the temperature range 200–500 °C in air. Impedance analysis has been used to separate contributions of grains, grain-boundaries and electrode–specimen interface to the total observed resistance.

3. Results and discussion

Compositions viz. $Ce_{0.925}Mg_{0.075}O_{1.925}$ (CML00), $Ce_{0.920}Mg_{0.070}La_{0.010}O_{1.925}$ (CML01), $Ce_{0.910}Mg_{0.060}La_{0.030}O_{1.925}$ (CML03), $Ce_{0.900}Mg_{0.050}La_{0.050}O_{1.925}$ (CML05), and $Ce_{0.850}La_{0.150}O_{1.925}$ (CML15) have been prepared by auto-combustion method. XRD patterns of various compositions after sintering are shown in Fig. 1. Absence of characteristic lines of constituent oxides in the patterns confirmed the formation of single phase. There is a slight shift in 2θ values from the corresponding 2θ values of undoped ceria. XRD data could be indexed on the basis of a cubic unit cell similar to CeO_2. Lattice constant for all the compositions was calculated using the program 'UNIT CEL'. Lattice parameter for all the compositions is given in Table 2. Lattice parameter is more than undoped ceria (5.4019 Å) for all the five compositions. The increase in lattice parameter is due to dissolution of lanthanum and magnesium in ceria as La^{3+} ions (1.16 Å) and Mg^{2+} ions (0.89 Å). Lattice parameter increases with the increase of La because La^{3+} is much bigger than Ce^{4+} while Mg^{2+} is not very much smaller than Ce^{4+}. Crystallite size (d) of sintered powder was calculated from X-ray line broadening using Scherrer's formula.

$$d = \frac{0.9\lambda}{\beta \cos\theta} \quad (3)$$

where β is the full width at half maximum (FWHM) intensity of a Bragg reflection excluding instrumental broadening, λ is the wavelength of the X-ray radiation and θ is the Bragg angle and β is taken for strongest Bragg's peak corresponding to $2\theta \sim 28^\circ$ for all the six samples. Crystallite size of sintered powder obtained from X-ray line broadening is given in Table 1. Density of sintered pellets was determined by Archimedes principle. Lattice parameter, theoretical and experimental density and percentage porosity for all the samples are given in Table 2. Density of compositions decreases with the increasing percentage of lanthanum.

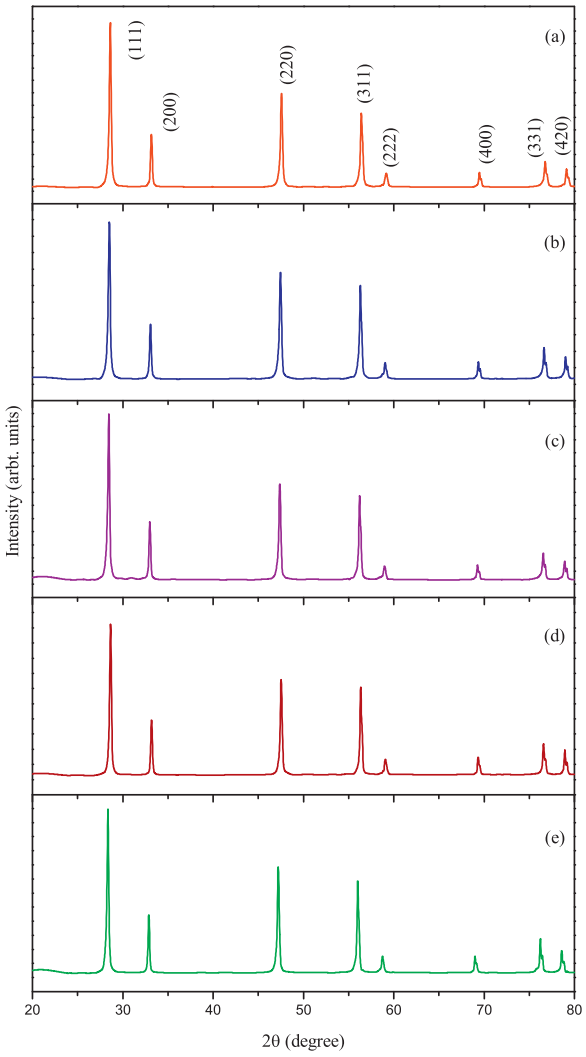

Fig. 1. Powder X-ray diffraction patterns of compositions: (a) CML00, (b) CML01, (c) CML03, (d) CML05 and (e) CML15.

Scanning electron micrographs for the sintered samples CML00, CML01, CML03, CML05, and CML15 are shown in Fig. 2. These show dense microstructure with distinct grains and grainboundaries.

Impedance measurements were performed in air in the temperature range 250–500 °C and in the frequency range 1 Hz to 1 MHz. Generally, in a complex plane impedance plot, three circular arcs are observed. The arc corresponding to contribution of grains passing through the origin is observed in the highest frequency range. The arc corresponding to grainboundaries is found in the intermediate frequency range. The third arc in the lowest frequency range corresponds to contribution of electrode–specimen interface.

Table 2
Lattice parameter, theoretical and experimental density and percentage porosity of CeO_2 and compositions CML00, CML01, CML03, CML05 and CML15.

Composition	Lattice parameter (Å)	Theoretical density (gm/cm^3)	Experimental density (gm/cm^3)	% porosity
[a]CeO_2	5.4019 ± 0.0016	7.2553	6.8926	5.0
CML00	5.4060 ± 0.0002	7.0092	6.6396	5.2
CML01	5.4146 ± 0.0001	6.8143	6.3246	7.1
CML03	5.4133 ± 0.0005	6.8666	6.4058	6.7
CML05	5.4218 ± 0.0002	6.8817	6.3794	7.2
CML15	5.4406 ± 0.0001	6.7721	6.2442	7.7

[a] Data taken from Ref. [22].

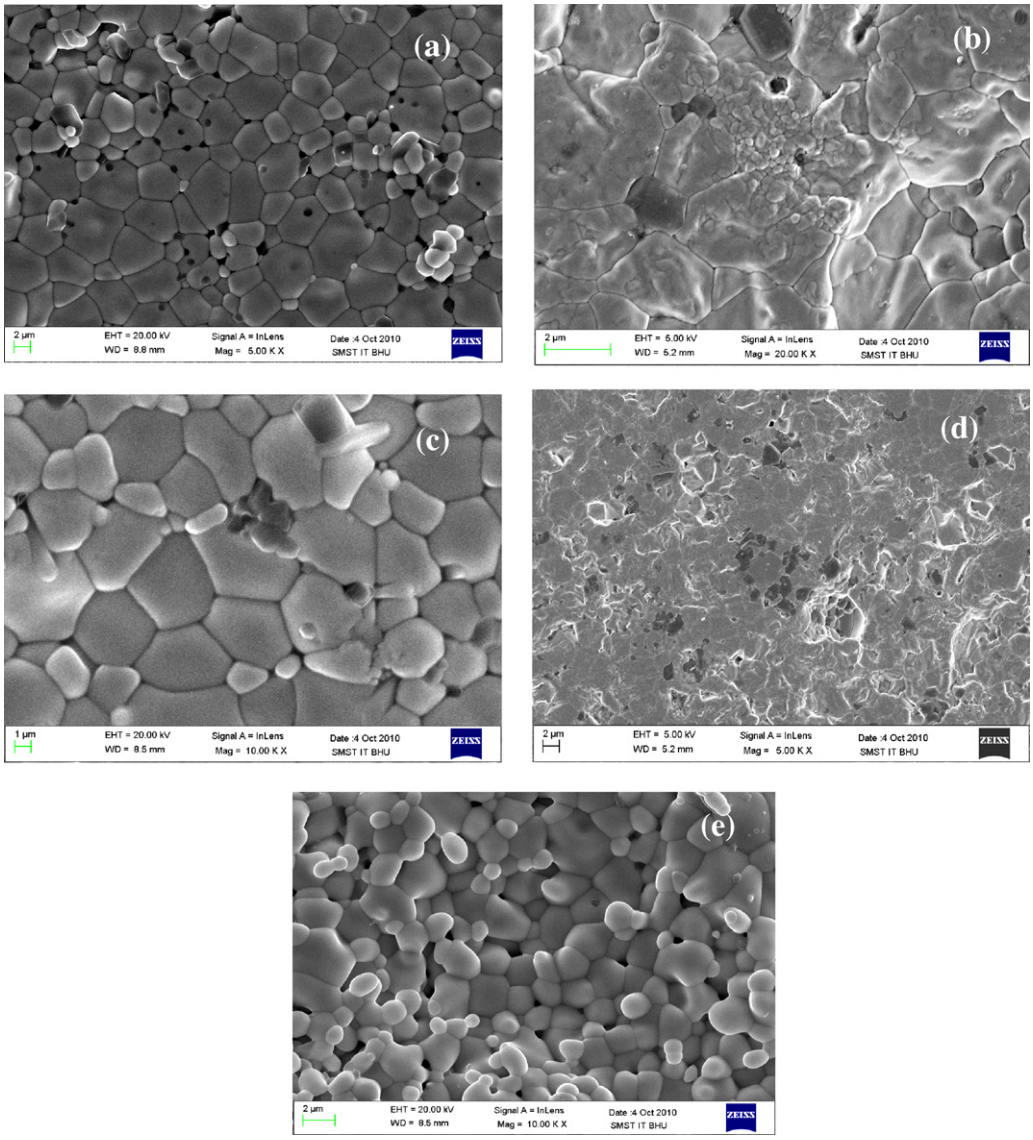

Fig. 2. Scanning electron micrograph of compositions: (a) CML00, (b) CML01, (c) CML03, (d) CML05 and (e) CML15.

Intercept of the arcs on the real axis represents the contribution of the grains, grainboundaries and electrode–specimen interface to the total observed resistance in order of decreasing frequency [19].

Complex plane impedance plots for CML00 at different temperatures are shown in Fig. 3(a–f). In case of CML00, a steep line passing through origin appears in the complex plane impedance plots below 300 °C. This is because of very high resistance of this sample up to these temperatures. However on plotting the data in the high frequency range on an expanded scale, the contribution of grains at these temperatures is clearly seen. With increasing temperature, a distorted arc is observed which can be fitted to three depressed arcs corresponding to contributions of grains, grainboundaries and electrode–specimen interface in order of decreasing frequency.

Complex plane impedance plots for CML01, CML03, CML05 and CML15 are essentially similar. Typical plots for CML03 are shown in Fig. 4(a–f). Two or three depressed circular arcs are observed depending on the temperature of measurement. With increasing temperature frequency range of these arcs shift to higher frequency side. Therefore, for compositions CML01, CML03, CML05 and CML15, the depressed circular arc corresponding to grains disappears completely above ~350 °C. Above 350 °C, the contribution of grains to the total resistance is given by the intercept on Z' axis to the left of higher frequency side of the arc due to grainboundaries.

Values of resistance of grains (R_g) and grainboundaries (R_{gb}) can be determined from the intercepts of these circular arcs with the real axis (Z'). The value of capacitance corresponding to grains and grainboundaries can be obtained from the frequency of the highest point in the corresponding arc where the relation $\omega RC = 1$ is satisfied. Here ω is the angular frequency, $\omega = 2\Pi f$, f is the applied frequency in Hz at arc maximum. Grains have capacitance of order of picofarad, grainboundaries have capacitance of order of nanofarad and electrode–specimen interface has capacitance of order of microfarad [20]. These values are of right magnitude for grains, grainboundaries and electrode–specimen interface.

Conductivity of the grains of the samples is determined using the relation

$$\sigma_g = \frac{1}{R_g} \times \frac{l}{a} \tag{4}$$

where σ_g is the conductivity of grains(bulk), R_g is the resistance of grains, l is the thickness and a is the area of pellet. Fig. 5 shows $\log \sigma_g T$ vs $1000/T$ plots of conductivity of grains for all the compositions. These plots are linear with a single slope in the entire

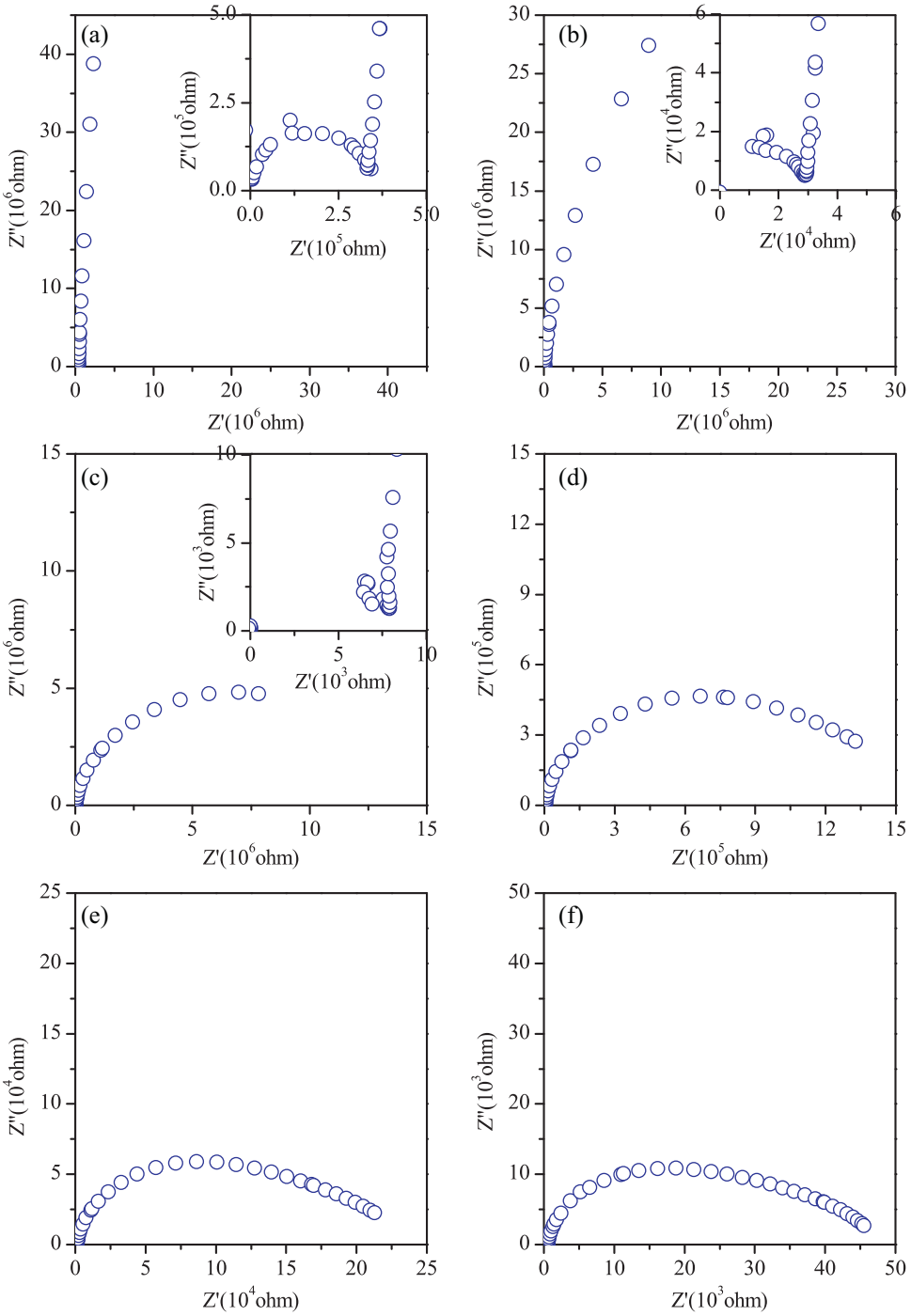

Fig. 3. Complex plane impedance plots of composition CML00 at a few temperatures: (a) 250 °C, (b) 300 °C, (c) 350 °C, (d) 400 °C, (e) 450 °C and (f) 500 °C in air.

temperature range of measurement. Values of activation energy for conduction in grains, E_g for all the compositions, determined from the plots, by least square fitting of the data in Fig. 5 are given in Table 3.

Conductivity of grainboundaries can be determined using the relation

$$\sigma_{gb} = \frac{1}{R_{gb}} \times \frac{D}{d} \times \frac{l}{a} \quad (5)$$

where R_{gb}, D, d, l and a are the resistance of grainboundaries, average thickness of the grainboundaries, average grain size, thickness of the pellet and area of the pellet respectively. The ratio D/d can be determined from the ratio C_g/C_{gb} where C_g and C_{gb} are the

Table 3
Activation energy of grains (E_g), grainboundaries (E_{gb}) and total activation energy (E_t) for compositions CML00, CML01, CML03, CML05 and CML15.

Composition	Activation energy of grains, E_g (eV)	Activation energy of grain boundaries, E_{gb} (eV)	Total activation energy, E_t (eV)
CML00	1.23	1.67	1.67
CML01	0.74	1.14	1.26
CML03	0.85	1.33	1.26
CML05	0.73	1.05	0.97
CML15	0.91	1.24	1.07

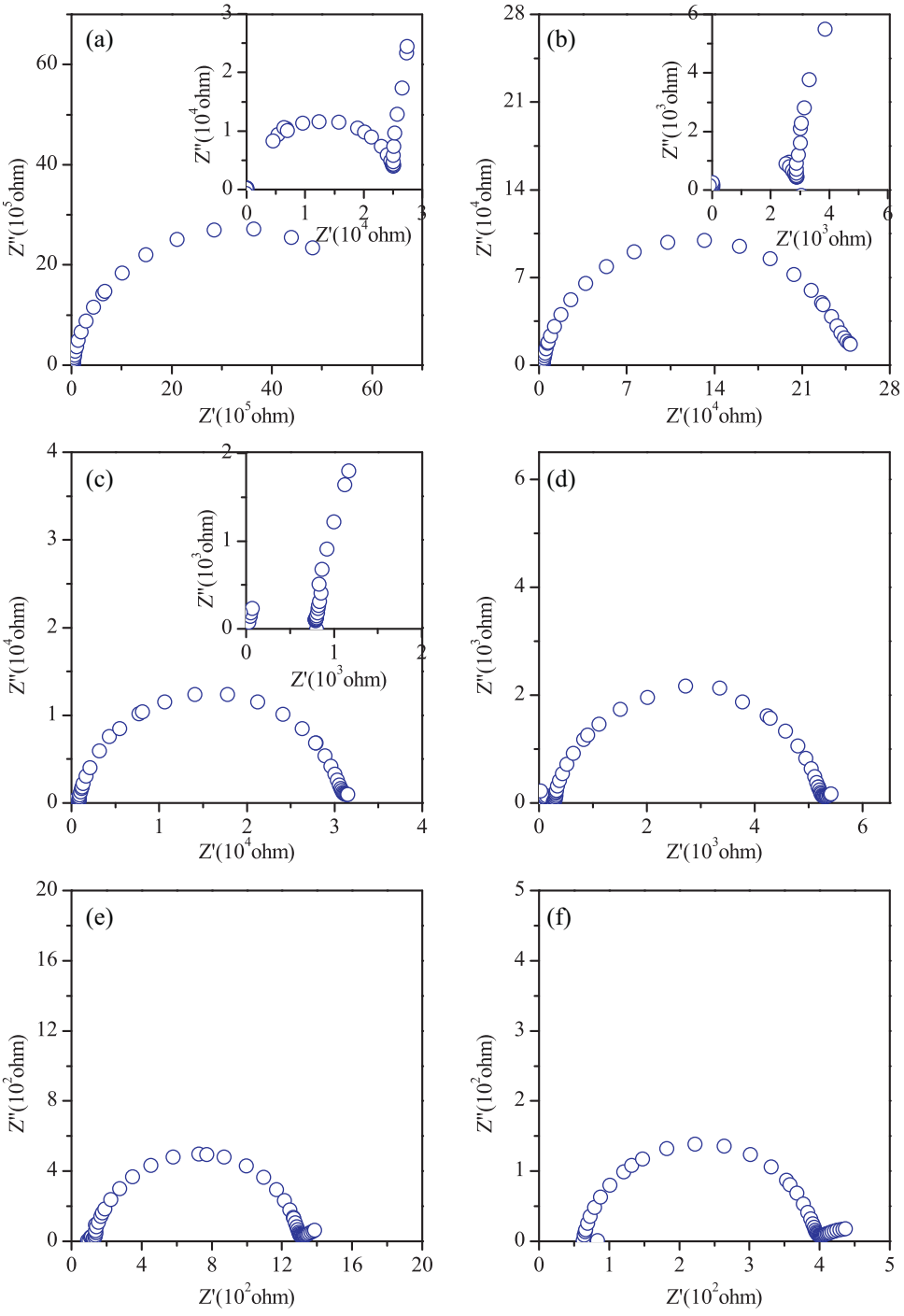

Fig. 4. Complex plane impedance plot of composition CML03 at a few temperatures: (a) 250 °C, (b) 300 °C, (c) 350 °C, (d) 400 °C, (e) 450 °C and (f) 500 °C in air.

capacitance of grains and grainboundaries determined from the peak point of the circular arcs in Z'' vs Z' plots [20]. However in the present case it is not possible to determine C_g because circular arc corresponding to contribution of grains disappears after a particular temperature for all the compositions. Therefore, σ_{gb} cannot be determined from the above relation. Hence conductance G_{gb} $(1/R_{gb})$ of grainboundaries is determined. Fig. 6 shows plots of $\log G_{gb}T$ vs $1000/T$ for all the compositions. These are linear with single slope in the entire temperature range of measurement. Values of activation energy of conduction for grainboundaries are given in Table 3.

Total resistance of the sample is given by $R_t = R_g + R_{gb}$ [19]. Total conductivity has been determined using the formula

$$\sigma_t = \frac{1}{R} \times \frac{l}{a} \tag{6}$$

where l is the thickness and 'a' is the area of the sample. Plots of $\log(\sigma_t \cdot T)$ vs $1000/T$ are shown in Fig. 7. A linear behavior is observed showing that these follow Arrhenius behavior

$$\sigma_t = \frac{\sigma_0}{T} \cdot \exp\left(-\frac{E_t}{k_B T}\right) \tag{7}$$

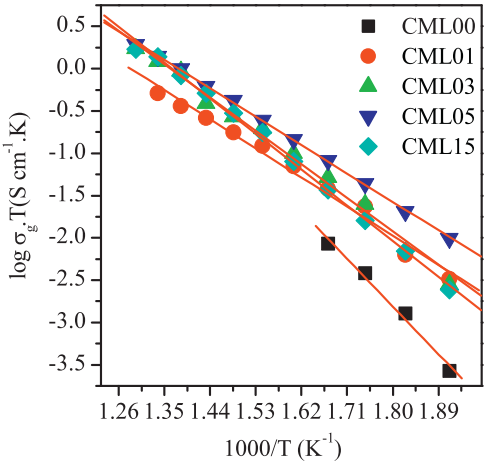

Fig. 5. Log $\sigma_g \cdot T$ vs 1000/T plot of compositions CML00, CML01, CML03, CML05 and CML15.

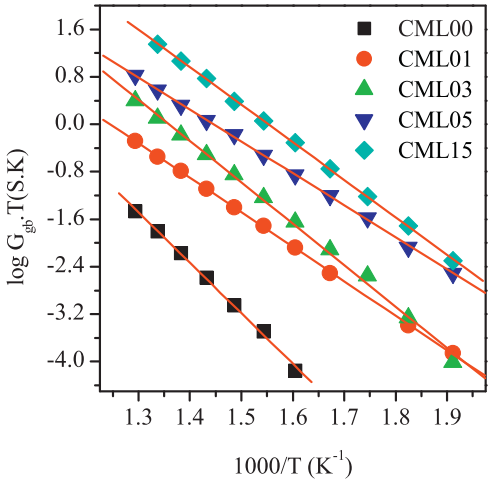

Fig. 6. Log $G_{gb} \cdot T$ vs 1000/T plot of compositions CML00, CML01, CML03, CML05 and CML15.

where T stands for temperature in K, k_B for the Boltzman constant, and σ_0 for a temperature-independent pre-exponential factor. Values of σ_0 are given in Table 4. Fig. 7 shows that the total conductivity increases with increasing concentration of La.

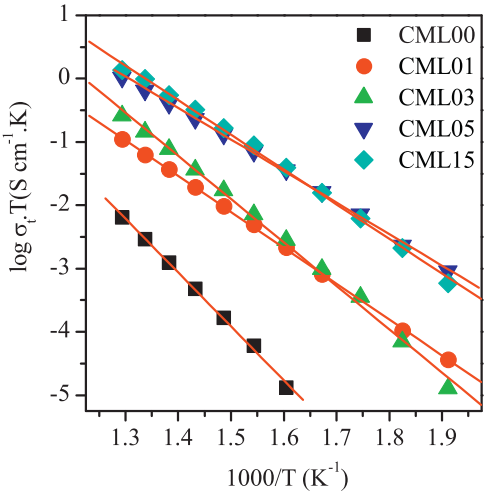

Fig. 7. Log $\sigma_t \cdot T$ vs 1000/T plot of compositions CML00, CML01, CML03, CML05 and CML15.

Table 4
Total conductivity σ_t at 700 °C, value of pre exponential factor σ_0 and value of effective index for the compositions CML00, CML01, CML03, CML05 and CML15.

Composition	[a]Total conductivity σ_t at 700 °C (S cm^{-1})	σ_0	Effective ionic index
CML00	3.11×10^{-4}	6.76×10^{8}	0.656
CML01	4.98×10^{-3}	2.45×10^{6}	0.683
CML03	1.19×10^{-2}	2.29×10^{8}	0.729
CML05	2.54×10^{-2}	2.88×10^{6}	0.765
CML15	5.14×10^{-2}	2.08×10^{7}	0.886

[a] Obtained by extrapolation.

Among all the compositions, composition with $x = 0.00$, $y = 0.15$ has the maximum lattice parameter. Therefore, more open structure seems to facilitate movement of the oxide ions. This increases the ionic conductivity. Therefore, CML15 exhibits the highest ionic conductivity. Values of activation energy of total ionic conductivity E_t for all compositions are given in Table 3. $Ce_{0.8}Sm_{0.2}O_{1.9}$ and $Ce_{0.8}Gd_{0.2}O_{1.9}$ have been reported to exhibit highest electrical conductivity among all the ceria-based oxides [21]. The total conductivity of $Ce_{0.8}Sm_{0.2}O_{1.9}$ and $Ce_{0.8}Gd_{0.2}O_{1.9}$ at 700 °C is 3.49×10^{-2} and 2.97×10^{-2} S cm^{-1}, respectively. In our investigation, CML15 and CML05 have shown comparable value of total conductivity at 700 °C (obtained by extrapolation) given in Table 4. Composition CML05 seems to be a promising candidate as a solid electrolyte for IT-SOFCs being cheaper than Sm or Gd doped ceria material.

Mori et al. [13] defined the effective index to explain the ionic conductivity of ceria-based systems and concluded that CeO_2-based systems reach the ideal fluorite structure for high oxide ion conduction when the effective index is close to 1. The effective index is given by the formula

$$\text{Effective index} = \left(\frac{\text{avg.}\, r_c}{\text{eff.}\, r_o}\right) \times \left(\frac{r_d}{r_h}\right) \quad (8)$$

where avg r_c is the average ionic radius of the cations, r_o is the effective radius of oxygen ion, r_d is the average ionic radius of the dopant, and r_h is the ionic radius of host cation. The effective oxygen ion radius is given by formula

$$\text{eff.}\, r_o = 1.4 \times \left[\frac{(2-\delta)}{2}\right] \quad (9)$$

where 1.4 Å is the ionic radius of O^{2-} in oxides and δ is the level of oxygen vacancies in CeO_2 based oxides. The effective index for different compositions is given in Table 4. Values given in Table 4 show that effective index of composition with $x = 0.00$, $y = 0.15$ is closest to 1 as compared to other four compositions. Therefore, the ionic conductivity of the composition with $x = 0.00$, $y = 0.15$ is maximum. It is concluded that ionic conductivity increases with an increase of the effective index confirming the validity of Mori's Criteria. There is no enhancement in conductivity due to co-doping with Mg and La.

4. Conclusions

Compositions in the system $Ce_{1-x-y}Mg_xLa_yO_{2-x-y/2}$ (CML) with $x = 0.075$, 0.070, 0.060, 0.050 and 0.000 and $y = 0.000$, 0.010, 0.030, 0.050 and 0.150 have been prepared by auto-combustion method successfully. All the compositions have fluorite type crystal structure similar to pure ceria. Value of lattice parameter is maximum for the $x = 0.00$, $y = 0.150$. Morphology of the samples shows homogeneous and dense microstructures. Total conductivity increases with increase in La content. CML05 seems to be a potential candidate for IT-SOFCs as it will be cheaper than the Sm or Gd singly or co-doped ceria. There is no enhancement in conductivity due to co-doping of Mg and La.

Acknowledgements

Thanks are due to Department of Science and Technology, New Delhi for financial support. One of the authors, Namrata Singh is thankful to University Grant Commission, New Delhi for providing a fellowship during the course of these investigations.

References

[1] H. Inaba, H. Tagawa, Solid State Ionics 83 (1996) 1–16.
[2] K. Eguchi, T. Setoguchi, T. Inoue, H. Arai, Solid State Ionics 52 (1992) 165–172.
[3] Y. Liu, B. Li, X. Wei, W. Pan, J. Am. Ceram. Soc. 91 (2008) 3926–3930.
[4] P.P. Dholabhai, J.B. Adams, P. Crozier, R. Sharma, J. Chem. Phys. 132 (2010) 094104.
[5] M. Mogensen, N.M. Sammes, G.A. Tompsett, Solid State Ionics 129 (2000) 63–94.
[6] A. Arif Ismail, J. James Hooper, J.B. Giorgi, T.K. Woo, PCCP 13 (2011) 6116–6124.
[7] C. Peng, Y.N. Liu, Y.X. Zheng, Mater. Chem. Phys. 82 (2003) 509–514.
[8] B.C.H. Steele, Solid State Ionics 129 (2000) 95–110.
[9] S. Banerjee, P. Sujatha Devi, Solid State Ionics 179 (2008) 661–669.
[10] T. He, Z. Lu, L. Pei, X. Huang, Z. Liu, W. Su, J. Alloys Compd. 333 (2002) 231–236.
[11] Y. Zheng, H. Gu, H. Chen, L. Gao, X. Zhu, L. Guo, Mater. Res. Bull. 44 (2009) 775–779.
[12] Y. Zheng, Y. Shi, H. Gu, L. Gao, H. Chen, L. Guo, Mater. Res. Bull. 44 (2009) 1717–1721.
[13] T. Mori, T. Ikegami, H. Yamamura, J. Electrochem. Soc. 146 (1999) 4380–4385.
[14] F.-Y. Wang, S. Chen, S. Cheng, Electrochem. Commun. 6 (2004) 743–746.
[15] S. Lübke, H.-D. Wiemhöfer, Solid State Ionics 117 (1999) 229–243.
[16] T. Shimonosono, Y. Hirata, Y. Ehira, S. Sameshima, T. Horita, H. Yokokawa, Solid State Ionics 174 (2004) 27–33.
[17] N.K. Singh, P. Singh, M.K. Singh, D. Kumar, O. Parkash, Solid State Ionics 192 (2011) 431–434.
[18] R.D. Shannon, Acta Crystallogr. A 32 (1976) 751–767.
[19] I.M. Hodge, M.D. Ingram, A.R. West, J. Electroanal. Chem. 74 (1976) 125–143.
[20] R. Gerhardt, A.S. Nowick, J. Am. Ceram. Soc. 69 (1986) 641–646.
[21] Y.-P. Fu, S.-H. Chen, J.-J. Huang, Int. J. Hydrogen Energy 35 (2010) 745–752.
[22] N.K. Singh, P. Singh, D. Kumar, O. Prakash, Ionics 18 (2012) 127–134.